Imaging critical fluctuations of pure fluids and binary mixtures

John J. Hegseth*
Department of Physics, University of New Orleans, New Orleans, Louisiana 70148, USA

Ana Oprisan†
Department of Physics and Astronomy, College of Charleston, Charleston, South Carolina 29424, USA

Yves Garrabos
ESEME, Institut de Chimie de la Matière Condensée de Bordeaux, UPR 9048, CNRS, Université de Bordeaux I, Avenue du Dr. Schweitzer, F-33608 Pessac Cedex, France

Daniel Beysens
Physique et Mécanique des Milieux Hétérogènes, UMR 7636 CNRS - ESPCI - Université Pierre et Marie Curie - Université Paris Diderot, 10 rue Vauquelin, 75005 Paris, France and Service des Basses Températures, CEA-Grenoble & Université Joseph Fourier, Grenoble, France
(Received 24 March 2014; revised manuscript received 29 May 2014; published 25 August 2014)

We use optical microscopy techniques to directly visualize the structures that emerge in binary mixtures and pure fluids near their respective critical points. We attempt to understand these structures by studying the image formation using both a phase contrast and a dark field filter to our microscope. We found that images of critical fluctuations for both liquid-liquid and liquid-gas critical systems have gray level intensity histograms with Gaussian shape. For all fluids investigated, the temperature-dependent standard deviation of the Gaussian histogram follows a power law with the same exponent. Since the image intensity fluctuations are determined by order parameter fluctuations, this direct imaging method allowed us to estimate the critical exponent of compressibility with very good accuracy.

DOI: 10.1103/PhysRevE.90.022127 PACS number(s): 05.40.−a, 05.70.Jk, 42.30.Kq, 42.30.Va

I. INTRODUCTION

When small changes are made to a system's thermodynamic state variables, the system responds by minimizing its free energy $F(T, X)$, where T is the temperature and X is a quantity that characterizes the system, such as density, magnetization, or concentration [1–3]. If this thermodynamic potential, $F(T, X)$, has two minima, then two phases coexist. When T changes, the free energy F may split from a potential with one minimum to a potential with two minima, i.e., $X(T)$ bifurcates at the point (T_c, X_c) and undergoes a continuous phase transition that leads to phase separation [4,5]. Such phase transitions are described by the order parameter $M = X - X_c$, which vanishes in the disordered state and is nonzero in the ordered state [2,6,7]. The order parameter M measures the system's ordering or its degree of symmetry. For pure fluids near their liquid-gas critical point, the order parameter is the density distance to the critical density [8]. For a binary mixture near their liquid-liquid critical point, the order parameter is the concentration distance to the critical concentration [9]. According to the order parameter theory of critical phenomena [2,10], far from the critical temperature T_c, the probability $p(M)dM$ for a small but macroscopic subsystem to have the order parameter M in the ranges M and $M+dM$ is

$$p(M)dM = A\exp\left[-\frac{1}{2}\left(\frac{\partial^2 F}{\partial M^2}\right)_0 \delta M^2 + \frac{1}{4}\left(\frac{\partial^4 F}{\partial M^4}\right)_0 \delta M^4 + O(\delta M^6)\right] dM, \quad (1)$$

where A is the normalization constant, F is the free energy of the system that was expanded about its minimum, and only the even powers are retained in the probability distribution function. For temperatures far from the critical point, the coefficient $(\partial^2 F/\partial M^2)_0$ is large and, as a result, the quadratic factor in Eq. (1) is dominant. Therefore the first approximation for the probability distribution function of fluctuations is Gaussian with the variance given by the compressibility $\chi \propto (\partial^2 F/\partial M^2)_0^{-1}$. As the temperature approaches its critical value, the compressibility scales as $\chi \propto \tau^{-\gamma}$, where $\tau = (T/T_c - 1)$ is the reduced temperature and γ is a universal exponent. For pure fluids, the experimental value of γ varies form 1.19 for H_2O [11] to 1.24 for CO_2, SF_6, Xe [12], and C_2H_4 [13]. (For a review of experimental values of γ, see [14].) From the renormalization group theory [15,16], the critical exponent value is $\gamma = 1.24$ [17].

Direct microscopic observations of fluctuations have previously been reported using spatially coherent light [9,18]. A detailed analysis of the direct imaging treatment used here was provided by Trainoff and Cannell [19]. In their seminal work, Trainoff and Cannell explained the mechanism of image formation through interference between the transmitted beam through the fluid and the phase and amplitude modulated scattered light by local variations of the refractive index.

*Present address: Department of Radiation Oncology, University of Louisville, 529 S. Jackson Street, Louisville, Kentucky 40202, USA.
†Corresponding author: oprisana@cofc.edu

The shadowgraph signal, i.e., the light intensity recorded by CCD camera, is proportional to the lateral fluctuations of the refractive index [20–22]. The refractive index fluctuations are subsequently related to concentration fluctuations near the liquid-liquid critical point [9,23] and to density fluctuations near the liquid-gas critical point [24,25], respectively. Here we use a shadowgraph method to direct image thermal fluctuations very close to the critical point. At the same time, the shadowgraph method is also extensively used for investigating nonequilibrium fluctuations. Since the first direct imaging of nonequilibrium fluctuations in a liquid mixture done by Vailati and Giglio [26], this experimental technique was refined and applied to many other nonequilibrium systems. The shadowgraph technique was recently used for imaging thermal and electrohydrodynamic convections in nematic liquid crystals [20], investigating Rayleigh-Bénard convection [27] (for a review see also [28]), and studying nonequilibrium concentration fluctuations, both on Earth [29,30] and under microgravity conditions [31].

Near T_c, large forward scattering from a fluid element interferes with the transmitted light at the imaging pixel to produce bright or dark intensity variations. We have observed large thermal fluctuations as T approaches T_c in several systems, such as the binary liquid of methanol and partially deuterated cyclohexane (CC*-Me) [32], an isobutyric acid and water (IW) binary mixture [33,34], and sulfur hexafluoride (SF_6) in weightlessness [32,35–37].

As suggested by Guenoun *et al.* [9] and proved by physical optics treatment of the quantitative shadowgraph technique [19,20,22], order parameter fluctuations δM induce fluctuations in the intensity of the scattered light with a corresponding Gaussian gray level intensities histogram similar to Eq. (1). For example, in binary mixtures near the critical point of miscibility, the order parameter fluctuation, i.e., the concentration fluctuations, induce small changes in the index of refraction that determine changes in the phase of scattered light. Exactly at the critical point (T_c, X_c), the second-order derivative of the free energy vanishes $[(\partial^2 F/\partial M^2)]_T = 0$ and the corresponding compressibility χ diverges. Near the critical point, the minimum of $F(T, M)$ is spread out over a wide range of values of the order parameter M [2,38]. The large spread δM that exists near the critical point leads to either extremely large (divergence) or vanishing values of some thermophysical properties of the system. Both equilibrium and transport properties behave according to universal power laws that either diverge to infinity or converge to zero at the critical point [4,6,39]. The singularities of some thermophysical properties could be related to domains of order parameter M that are statistically self-similar at the critical temperature T_c. For example, density fluctuations are self-similar since they exist at all length scales at the critical point such that the fluctuation correlation length diverges at T_c according to $\xi = \xi_0 \tau^{-\nu}$, where ξ_0 is a system-dependent correlation amplitude and ν is a universal exponent [24,40,41]. The increase in the fluctuation correlation size near $M = 0$ manifests by an increase of the scattered light intensity. When the fluctuations of the order parameter δM are correlated over a size comparable to the wavelength of light, the scattering from the media greatly increases. Light scattered from the correlated fluctuations coherently interfere to produce a striking visual effect called the critical opalescence [42–45]. This strong correlation between the intensity of the scattered light and the fluctuations of the order parameter allows the properties of near critical fluids to be probed with light-scattering techniques [46–50].

Precise measurements of diverging thermophysical properties near a second-order phase transition are severely hindered by the influence of the gravitational field. For example, in pure fluids, such as SF_6, the gravitational field leads to fluid stratification due to the divergence of isothermal compressibility near the critical point [17,51]. To overcome these challenges, three experimental strategies were developed. One approach considered shrinking the vertical size of the sample cells for ground-based experiments in order to minimize the effect of the gravitational field [4,5,52]. The drawback is that the finite size effects then limit the accuracy of the measured thermophysical properties [53,54]. Another approach is to reduce the influence of the gravitational field by taking advantage of the microgravity environment, usually of the order of 10^{-4} g, in a low-Earth-orbiting spacecraft or long-term space station missions [55]. Since the first low-gravity experiment on phase separation in liquid binary mixtures and pure fluids [23], advances in both the duration and the accuracy of measurements allowed more precise estimation of critical exponents. (For a review see [55].) A third strategy, that can only be applied to some binary mixtures, is density matching. It consists in deuterating the lighter component of the mixture so as to approximately match the molar mass of the heavier component. This strategy was successfully used to significantly reduce the stratification due to gravity [9,56,57].

II. EXPERIMENTAL SETUP

There are two parts to the experimental setup: an optical microscope, which allowed us to use three different light-filtering methods to investigate density fluctuations, and a thermostat that enclosed the sample cell filled out with a fluid near the critical point. The optical microscope setup described below was only used for investigating the fluctuations near liquid-liquid critical points on Earth in deuterated cyclohexane-methanol and in isobutyric acid-water systems. Thermal fluctuations near liquid-vapor critical point in sulfur hexafluoride were investigated in microgravity using the optical microscope included with ALICE 2 instrumentation. (For details regarding the microgravity optical setup see [37,58].)

A. Optical microscopy setup for ground-based experiments

The sample cell is placed near the focal point of L_3 and its position is adjusted with a translation stage so that the field of view is near the output window of the cell. This also allowed us to properly position the object to form an image on a CCD camera (Sony XC-75CE with 752 × 582 pixels) approximately 1 m from L_3. The optical resolution in the object plane is of the order of 1 μm, comparable to both the diffraction resolution $\approx$0.5 μm and the fluid element resolution $\approx$2.2 μm. We used a wide-band light source, a 100-W halogen lamp, which gave a small coherence time and a corresponding longitudinal coherence length of $\approx$1 μm. The geometry of our optical setup gave a spatial coherence of $\approx$120 μm in

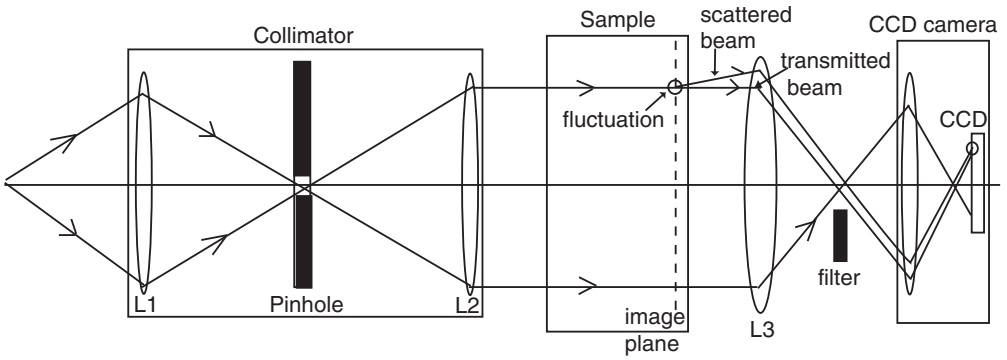

FIG. 1. Schematic representation of the optical microscopy system (not at scale). A white light source and a collimator produced a parallel beam of light after passing through a 0.8-mm pinhole with two 50-mm lenses, L_1 and L_2. This light scattered by fluctuations in the turbid media is collected by a high-quality, 50-mm photographic lens L_3 (Olympus, OM). An image of the fluid is formed on the CCD camera that is $\approx$1 m from L_3.

the object's plane. Since our microscopic field of view was $\approx$1.5 mm, it corresponds to a spatial coherence of over 8% of the field of view, or 46 $\times$ 46 pixels, on the CCD image plane.

In order to conveniently use the optical microscopy system schematically represented in Fig. 1, we have designed a thermal control system that used air convection and radiation for heat transfer. The cell was temperature controlled by placing it near the center of an aluminum cylinder with a diameter of 10 cm and height of 18 cm that had a foil heater glued to its exterior. Two holes in the heating cylinder, which were aligned with the optical axis of the cell, allowed light to pass through the sample fluid. To prevent convective cooling of the sample cell windows, these holes are closed at both ends with optical windows. Two more thermal shields made of 7-cm-thick polystyrene surrounded the heating cylinder and provided a constant ambient temperature for the inner cylinder. We placed the entire system containing the cell, the heating cylinder, and the thermal shields on an optical bench (see Fig. 1).

III. DIRECT VISUALIZATION OF FLUCTUATIONS NEAR LIQUID-LIQUID CRITICAL POINT

A. Partially deuterated cyclohexane and methanol system

The sample cell used with the above-described optical system (see Sec. II) was filled out with a binary mixture of partially deuterated cyclohexane and methanol (CC*-Me) [32]. This sample cell was prepared by mixing the two chemical substances such that the concentration of cyclohexane was at a well-known critical concentration $c_c = 71\%$ by weight or mass fraction [42,57]. To reduce sedimentation, we have density matched the mixture of CC*-Me. This mixture was placed between two sapphire windows with a 10-mm diameter and 8.5-mm thickness each, separated by a gold-coated 3-mm-thick brass spacer. This sample cell was placed in a larger, 6-cm diameter and 6-cm length, copper housing. Although the sample cell was filled out to a slightly off-critical concentration, $c = (cc - 0.01) \pm 0.002$, it is well within the concentration range $|c - c_c| < 0.05$, where fluctuations are visible as in Guenoun *et al.* [9].

The CC*-Me system exhibits the critical behavior when the temperature and concentration are near the critical point in the (T, c) space, where c is the concentration of one of the chemical species [57]. Depending on its temperature T, the system mixes or phase separates. The order parameter of the binary mixture CC*-Me is $M = c - c_c$. Although the CC*-Me system allowed the density to be precisely matched, when quenched below $T_c = 46.64^\circ C$, slow sedimentation of the phase-separated droplets were clearly visible in the microscopic field of view after several hours. At the beginning of the experiment, the sample cell was first mechanically shaken by hand and was subsequently heated above T_c to approximately 50°C, where the binary fluid was allowed to sit for at least 12 hours so that it was thoroughly mixed by diffusion. The temperature of the sample cell was then decreased towards the critical point in steps or temperature quenches, ΔT. As we approached T_c, finer temperature quenches were used. Far from T_c, the thermal quench was $\Delta T = 1$ K, whereas closer to T_c, we used a thermal quench of $\Delta T = 1$ mK. The thermal control system achieved stability as high as 0.1 mK over 12 hours and was mostly limited by the room temperature variations.

We have applied several filters to the light as shown in Fig. 1. Images with no filter in the focal plane of L_3 are called *bright field* (BF) images [9,18,59]. The first filter, called *phase contrast* (PC), consisted of a mica quarter-wave-plate of 1 cm diameter [60–62]. This corresponds to about 4% of the lens area, or an angle of 0.1 radians for output light. The light that passed through the quarter-wave-plate was, over the broad band of optical wavelengths, phase delayed relative to what it would have been had it not passed through it. The light that focused on the quarter-wave-plate is the transmitted light, i.e., the part of the incoming parallel light wave not significantly scattered by fluctuations. The light that does not pass through the quarter-wave-plate was scattered by fluctuations and is not phase delayed. A phase object that only changes the phase and not the amplitude of the light, e.g., no energy absorption, would produce no net intensity change at the detector, because the phase information does not contribute to the magnitude of the wave measured at the detector. By phase delaying the transmitted light at the lens' output focal plane with respect to the scattered light, the wave at the detector is decomposed into two parts that may have a relative phase shift, making phase objects visible. The transmitted and scattered waves superpose

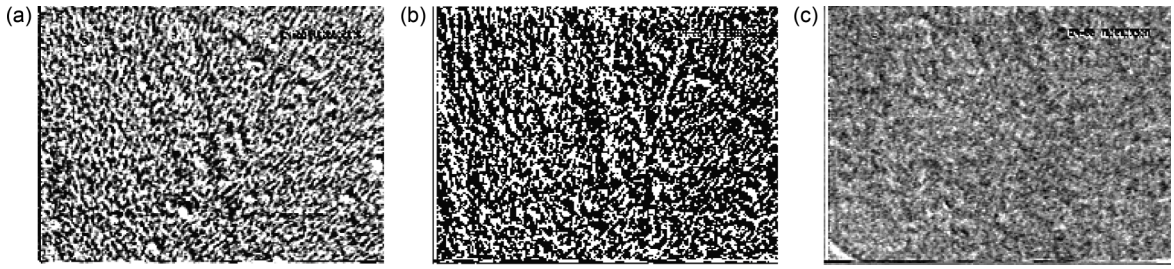

FIG. 2. Enhanced bright field (a), phase contrast (b), and dark field (c) images taken at approximately 1 mK above the critical temperature. The images are single frames extracted from video recorded at 25 frames/s and the correlation length at this temperature was ≈ 1 μm. The height of the image is 1.5 mm.

constructively or destructively so that their magnitude at the detector has an intensity variation that encodes a phase variation [59,62].

The second filter, called *dark field* (DF), used a 7-mm-diameter opaque disk, placed at the output focal point of L_3 to block the transmitted beam and only allowed the scattered light to enter the CCD array [63]. Both PC and DF filters were positioned at the focal plane using the same support. The plane of this support was perpendicular to the optical axis and was connected to another translation stage. This stage allowed the support to be displaced perpendicularly to the optical axis such that the light passed through the focus point unaltered in the case of the BF setup, the light near the focus point passed through the quarter-wave-plate in the case of the PC setup, and the light was blocked at the focus by the opaque disk in the case of the DF setup. Our optical setup allowed the three optical techniques (BF, PC, and DF) to be changed *in situ* by adjusting the translation stage (see Fig. 1).

The critical temperature was experimentally obtained by observing the phase separation process that for this system is a relatively quick process. The critical point was measured to within 0.5 mK with 1-mK quenches by observing the image after each quench to see if the fluid separated. The identification of the phase-separating features in the images was verified by waiting for over 12 hours at $T_c + 0.5$ mK. We identified the critical temperature as the last temperature quench for which the images retained the same characteristics and the fluid did not phase separate. After each quench, the temperature was allowed to equilibrate for at least 20 min before recording images of the fluctuations.

Above the critical temperature ($T > T_c$), we observed featureless images through our microscope. As T approaches T_c, we have observed images that exhibit spatial regions of varying light intensity. Figures 2(a)–2(c) show single frames extracted from video recordings with a frame rate of 25 frames/s taken above and close to the critical temperature T_c.

The original BF and PC images produced by our system were not of uniform intensity due to system noise from dust, etc. Optical noise produced nonuniform background intensity in addition to the intensity from density fluctuations. To correct for the optical system noise, we subtracted an image that was time-averaged over 1 min of video recording at a given temperature. This ensured that the local intensity fluctuations in the images did not contribute to the background as they averaged to negligible intensity variations and the noise was constant. The DF images were less sensitive to optical noise due to the inherent Fourier filtering that removed the low wave number components. The BF [Fig. 2(a)] and PC [Fig. 2(b)] images have their intensity shifted as described above and their contrast enhanced so that the spatial regions can easily be seen. Figure 2(c) shows a DF image. All three images shown in Fig. 2 were taken in sequence at the same temperature by recording 1 min of video, moving the translation stage to another filter, and repeating the procedure.

The purpose of the CC*-Me measurements was to test the Gaussian nature of the statistics of the images, so that only a single temperature above T_c was measured, namely, $T = T_c + 1$ mK. Figure 3 shows the distribution of intensity, or the histogram, for our 8-bit black and white digitized images, which resulted in 256 possible intensity levels at each pixel. The spatial sampling of light performed by the CCD camera produces $752 \times 582 = 437\,664$ possible pixels to distribute over these 256 intensity values and the vertical axis of the histogram is the number of pixels that have a given intensity value.

The small differences between the BF and PC intensity distributions are probably caused by a slight attenuation of the light from the mica wave-plate that is slightly opaque, the wave-plate edges, and the mounting piece for the wave plate. The DF image in Fig. 2(c) appears different from the PC and BF

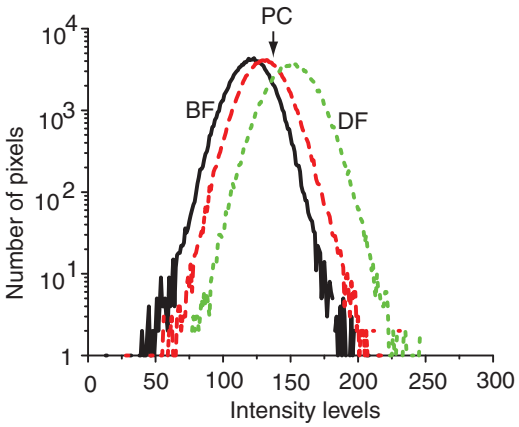

FIG. 3. (Color online) Log-linear plot of intensity distributions (histograms) of de-noised BF, PC, and DF images. The slight deviation from a Gaussian distribution is most likely determined by optical noise. The horizontal axis corresponds to the 256 intensity levels of the 8-bit images. The standard deviations of the three PDFs are 19.8 for BF, 20.3 for PC, and 22.8 for DF.

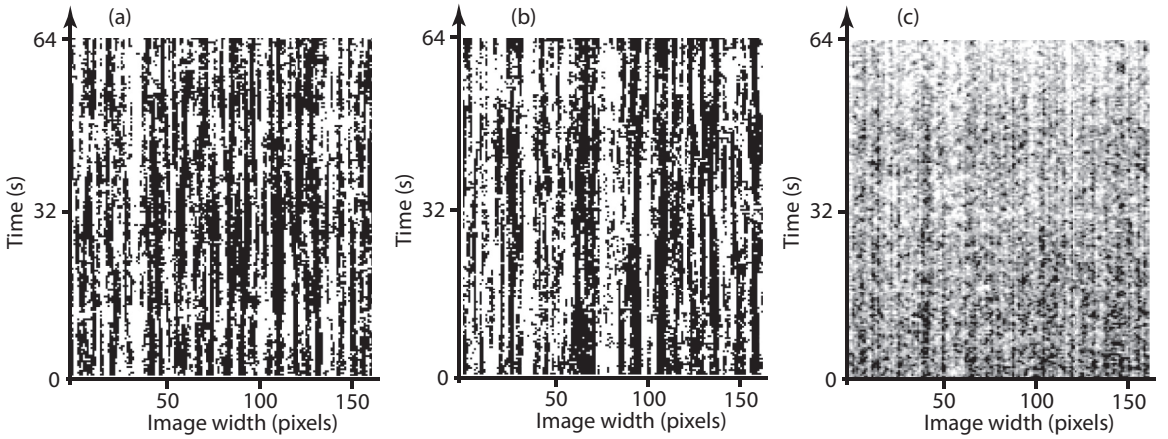

FIG. 4. Temporal evolution of the intensity of a line of pixels. The BF (a) and PC (b) images show a slow evolution superposed over a fast evolution. The DF (c) image only shows the fast evolution. The long temporal persistence of fluctuations in both BF and PC images is lost in the DF image, presumably because the fluctuations are in the low-q range that is filtered out in DF.

images. The intensity distributions shown in Fig. 3, however, reveal no substantial differences, i.e., all three exhibit Gaussian statistics to a good approximation. Because the transmitted part is blocked or masked from arriving at the CCD, we needed to increase the DF image signal substantially above the noise level. We accomplished this by increasing the incident light intensity by a factor of 4.8 by increasing the power to the light source.

We also recorded the temporal evolution of the intensity fluctuations. Figure 4 shows several examples of the temporal evolution of a line of pixels. These "waterfall" images of BF, PC, and DF show a horizontal display of the intensity of a line of fluid elements that change over time along the vertical axis. In the DF images, the large, slow regions are absent and the smaller regions last for only 1–2 s or a period that is almost 10 times less than the large regions in the BF and PC images. This suggests that the correlation time is significant for low q, i.e., a large spatial extent; fluctuations are present in both the BF and PC images and are completely filtered out in the DF images.

B. Isobutyric acid and water system

In our experiments, the IW system was not density matched, so that the fluctuations were observed near the cell's center using a density gradient technique [64]. A mixture of isobutyric acid and water was prepared at the critical concentration by weighing highly purified components directly into the experimental cell to minimize the relative error of c and c_c to approximately $10-2$. The cell was made of two, parallel, 20-mm-diameter fused quartz windows separated by a 2.00-mm spacer. This IW-filled sample cell was immersed in a water bath that allowed for a temperature stability of ± 0.2 mK over several hours.

The probability distribution of light intensities [Fig. 5(a)] was also Gaussian in the case of the IW mixture. As in the above CC*-Me case, the contrast of the image increased as T_c was approached, corresponding to an increase in the widths of the intensity distributions.

The temperature variation of the standard deviation Δ of the above Gaussian distribution [see Fig. 5(b)] reveals a power law scaling. In our experiments, the temperature range was limited

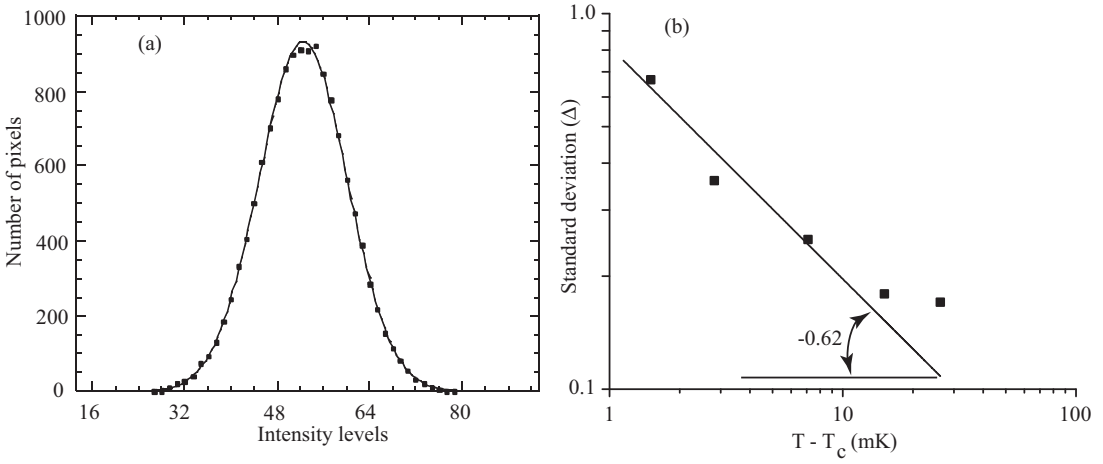

FIG. 5. (a) Intensity distributions (histograms) for the fluctuation images of isobutyric acid and water mixture at $T - T_c = 1$ mK. The curve is the best fit to a Gaussian distribution (continuous line). (b) Temperature dependence of the standard deviation Δ of the Gaussian distribution reveals a power law with an exponent of $\gamma/2 = 0.62$.

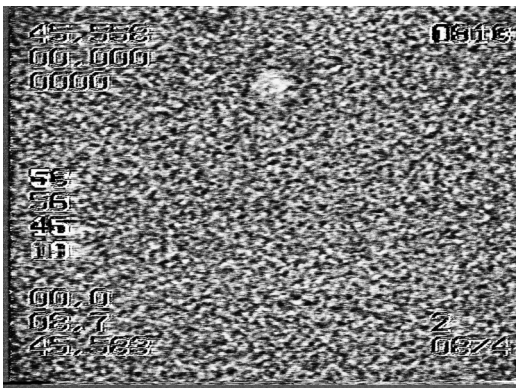

FIG. 6. Optical microscopy imaging reveals large density fluctuations in SF_6 fluid under reduced gravity very close to its critical point ($T - T_{cx} = 10\ \mu$K). The height of the image is 1 mm.

to about 1–30 mK because of a background noise that could not be eliminated by the above-described image subtraction method. For the isobutyric acid and water liquid mixture, Δ was fitted to

$$\Delta = a\,\tau^{-x}, \tag{2}$$

where $T_c = 299$ K for IW. Because the intensity fluctuations are determined by order parameter fluctuations [9], the variance Δ^2 of the Gaussian distribution of gray level intensities should follow the same scaling law as the compressibility $\chi \propto \tau^{-\gamma}$. As a result, we expect a scaling exponent of $x = \gamma/2 = 0.62$ for Δ. When both a and x were free parameters in Eq. (2), we obtained the dimensionless coefficient $a = 0.029 \pm 0.003$ and $x = 0.58 \pm 0.1$, with an adjusted $\chi^2 = 0.003\ 44$ and an adjusted coefficient of determination $R^2 = 0.918$. When the exponent x is fixed at 0.62, we obtained a slightly better fit with $a = 0.030 \pm 0.002$, an adjusted $\chi^2 = 0.002\ 71$, and an adjusted coefficient of determination $R^2 = 0.936$ [see Fig. 5(b)]. Our experimental results are in agreement with the prediction based on the thermodynamic fluctuation theory and allowed the estimation of the critical exponent γ through direct imaging of near critical fluctuations. We found that the standard deviation Δ of the Gaussian distribution of gray levels scales as the square root of the compressibility $\sqrt{\chi} \propto \tau^{-\gamma/2}$.

IV. DIRECT VISUALIZATION OF FLUCTUATIONS NEAR THE LIQUID-VAPOR CRITICAL POINT

The experiments with sulfur hexafluoride (SF_6) were performed with the ALICE 2 facility that was designed for operation in the weightlessness of a space vehicle to eliminate sedimentation. (For details regarding the optical setup and thermal stability parameters, see [36,37,65,66].) Here, we report data obtained with SF_6 near its critical density. A 3-mm-thick layer of SF_6 was enclosed in a copper beryllium cylindrical cell closed with two sapphire windows of 12 mm diameter. Using the microscopy of the ALICE 2 facility (see [37,58,67] for details), images of the fluid were obtained with a spatial resolution of 1.64 μm (a fluid element imaged into a CCD pixel). The depth of focus was approximately 5 μm and the microscope could be focused either on the middle plane of the cell or on a plane close to the cell's wall. No qualitative differences were observed between these two imaging planes. The cell was set in a thermostat with a precision of approximately 3 μK in the temperature range 25–70°C. We used controlled temperature steps as small as 100 μK [37,58,67]. The average density of the sample was determined within an accuracy of 0.1% by the method discussed in Ref. [65]. In our experiments, the density was $\rho/\rho_c = 1.009 \pm 0.001$. A precise determination of the critical temperature under weightlessness was performed automatically by recording the change of a 630-nm laser light's transmittance through the sample. In terms of reduced temperature, this density mismatch corresponds to $T - T_c = 30\ \mu$K. The fluctuations visible in Fig. 6 were observed at $10 \pm 3\ \mu$K above the coexistence temperature T_{cx}.

As in the previous section, the images were corrected for noise from the spatial response of the camera, the

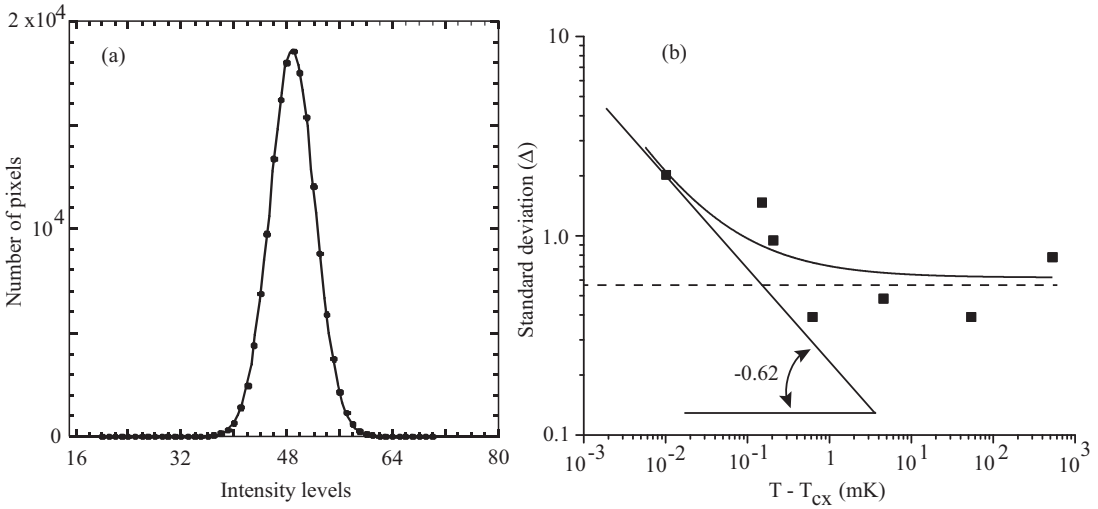

FIG. 7. (a) Intensity distributions (histograms) for the fluctuation images of SF_6 at $T - T_{cx} = 10\ \mu$K. The curve is the best fit to a Gaussian distribution (continuous line). (b) Temperature dependence of the standard deviation Δ of the Gaussian distribution reveals a power law with the exponent of $\gamma/2 \approx 0.62$.

inhomogeneity of the incident light, dust on the windows, etc. Since the modulation by the fluctuations was small compared to the average intensity, we subtracted a background image taken under the same conditions but at a higher temperature ($T - T_c = 0.3$ mK) where the fluctuations were no longer visible. We stress that the fluctuations at $T - T_{cx} = 10\ \mu$K are not domains formed by a phase separation process because the pattern did not grow during the 1-h observation time, which is about 2500 times longer than the fluctuation lifetime $t_\xi \approx 1.4$ s. The histogram, or intensity distribution, for SF_6 light intensity fluctuations fits well with a Gaussian function [continuous line in Fig. 7(a)].

The temperature variation of the standard deviation Δ was small in the temperature range 0.01–0.3 mK where fluctuations are visible. This temperature range was markedly smaller than for the IW mixture. We fitted the data to the same function as in Eq. (2),

$$\Delta = a\,\tau^{-x} + b, \tag{3}$$

with $T_c = 318.71$ K for SF_6, and a background constant $b = 0.53 \pm 0.1$ determined with data where fluctuations are not visible ($T - T_c > 0.3$ mK). Imposing the same value of the background $b = 0.53$ in the fit of all data, we found the free parameters $x = 0.43 \pm 0.15$ and the dimensionless fitting coefficient $a = 0.001 \pm 0.001$ with a reduced $\chi^2 = 0.096\ 28$ and an adjusted coefficient of determination $R^2 = 0.746$. We also fitted the data with a fixed exponent $x = 0.62$ and obtained $a = 0.000\ 11 \pm 0.000\ 02$ with a reduced $\chi^2 = 0.10095$ and an adjusted coefficient of determination $R^2 = 0.733$ [see Fig. 7(b)]. Similar to our experimental results regarding isobutyric acid and water liquid mixtures (Sec. IIIB), we also found that the standard deviation of the Gaussian fluctuation of light intensity for pure SF_6 in weightlessness obeys a power law [see Eq. (3)] with an exponent that is close to the theoretically predicted value of $\gamma/2 \approx 0.62$.

V. CONCLUSIONS

Ground-based experiments using optical microscopy allowed direct imaging of thermal fluctuations near the liquid-liquid critical point of two mixtures: isobutyric acid-water (IW) and deuterated cyclohexane-methanol (CC*-Me). We also carried out one microgravity experiment using ALICE 2 instrumentation to directly image fluctuations near the liquid-gas critical point of sulfur hexafluoride (SF_6). The critical behavior of both liquid-liquid and liquid-gas systems is determined by a second-order phase transition and they belong to the same universality class as the three-dimensional Ising model [9,17,24,52,53]. Following Guenoun *et al.* [9], we investigated the distribution of gray level intensities, i.e., image histograms, for the above near critical systems. Based on the thermodynamic theory of fluctuations, we expected that the probability distribution of order parameter fluctuations, $p(M)dM$, is Gaussian with a variance proportional to the system's compressibility, $\chi \propto (\partial^2 F/\partial M^2)_0^{-1}$. Since the image intensity is determined by the order parameter fluctuations [9], here we used the intensity histogram to estimate the temperature dependence of the variance of $p(M)dM$, i.e., the thermodynamic compressibility. Near the critical point, the compressibility scales as $\chi \propto \tau^{-\gamma}$, where $\tau = (T/T_c - 1)$ is the reduced temperature [4,17,24,66,68]. As a result, the standard deviation Δ of gray level histograms should scale as the square root of compressibility, i.e., $\Delta \propto \tau^{-\gamma/2}$, where $\gamma = 1.24$ [8,14,24].

Our experimental results are in agreement with the above prediction based on the thermodynamic fluctuation theory and allowed the estimation of the critical exponent γ through direct imaging of fluctuations. Indeed, we found experimentally that near the critical point the standard deviation of the Gaussian histograms followed power laws with respect to the reduced temperature.

ACKNOWLEDGMENTS

This work was supported by NASA Grants No. NAG3-1906 and No. NAG3-2447 to J.J.H. J.J.H. also gratefully acknowledges CNRS support. A.O. acknowledges a research and development grant from the College of Charleston. Y.G. and D.B. acknowledge CNES support. The authors are grateful to the anonymous reviewers for their valuable comments and suggestions that helped us improve the quality of the paper.

[1] N. Goldenfeld, *Lectures on Phase Transitions and the Renormalization Group* (Perseus Publishing, New York, 1992).
[2] L. D. Landau and E. M. Lifshitz, *Statistical Physics* (Butterworth-Heinemann, Oxford, 1980).
[3] F. Perrot, P. Guenoun, T. Baumberger, D. Beysens, Y. Garrabos, and B. Le Neindre, Phys. Rev. Lett. **73**, 688 (1994).
[4] H. E. Stanley, *Introduction to Phase Transitions and Critical Phenomena* (Oxford University Press, Oxford, 1987).
[5] C. Domb, *The Critical Point: A Historical Introduction to the Modern Theory of Critical Phenomena* (Taylor and Francis, Ltd., London, 1996).
[6] R. Botet and M. Plstrokoszajczak, Phys. Rev. E **62**, 1825 (2000).
[7] R. A. Ferrell and D. J. Scalapino, Phys. Rev. Lett. **29**, 413 (1972).
[8] Y. Garrabos, J. Phys. France **47**, 197 (1986).
[9] P. Guenoun, F. Perrot, and D. Beysens, Phys. Rev. Lett. **63**, 1152 (1989).
[10] L. P. U. Kadanoff, *Statistical Physics: Statics, Dynamics and Renormalization* (World Scientific, Singapore, 2000).
[11] J. V. Sengers, in *Phase Transitions, Status of the Experimental and Theoretical Situation*, edited by M. Lévy, J. C. Le Guillou, and J. Zinn-Justin (Plenum Press, New York, 1982), p. 95.
[12] R. Hocken and M. R. Moldover, Phys. Rev. Lett. **37**, 29 (1976).
[13] J. R. Hastings, J. M. H. Levelt Sengers, and F. W. Balfour, J. Chem. Thermodyn. **12**, 1009 (1980).
[14] J. Sengers and J. Shanks, J. Stat. Phys. **137**, 857 (2009).
[15] K. G. Wilson, Phys. Rev. B **4**, 3174 (1971).
[16] K. G. Wilson, Phys. Rev. B **4**, 3184 (1971).

[17] D. Beysens, J. Straub, and D. J. Turner, in *Fluid Sciences and Materials Science in Space*, edited by H. U. Walter (Springer, Berlin, 1987), p. 221.
[18] P. J. Debye and R. T. Jacobsen, J. Chem. Phys. **48**, 203 (1968).
[19] S. P. Trainoff and D. S. Cannell, Phys. Fluids **14**, 1340 (2002).
[20] S. Rasenat, G. Hartung, B. L. Winkler, and I. Rehberg, Exp. Fluids **7**, 412 (1989).
[21] M. A. Dominguez-Lerma, G. Ahlers, and D. S. Cannell, Phys. Rev. E **52**, 6159 (1995).
[22] G. S. Settles, *Schlieren and Shadowgraph Techniques: Visualizing Phenomena in Transparent Media* (Springer, Heidelberg, 2001).
[23] D. Beysens, P. Guenoun, and F. Perrot, Phys. Rev. A **38**, 4173 (1988).
[24] C. Domb, *Phase Transitions and Critical Phenomena* (Academic Press, New York, 2000).
[25] D. Beysens and Y. Garrabos, in *Space Station Utilisation*, edited by T.-D. Guyenne (ESA Special Publication, Darmstadt, Germany, 1996), p. 647.
[26] A. Vailati and M. Giglio, Nature (London) **390**, 262 (1997).
[27] J. R. de Bruyn, E. Bodenschatz, S. W. Morris, S. P. Trainoff, Y. Hu, D. S. Cannell, and G. Ahlers, Rev. Sci. Instrum. **67**, 2043 (1996).
[28] E. Bodenschatz, W. Pesch, and G. Ahlers, Annu. Rev. Fluid Mech. **32**, 709 (2000).
[29] F. Croccolo, D. Brogioli, A. Vailati, M. Giglio, and D. S. Cannell, Ann. N.Y. Acad. Sci. **1077**, 365 (2006).
[30] A. Oprisan, S. A. Oprisan, and A. Teklu, Appl. Opt. **49**, 86 (2010).
[31] A. Vailati, R. Cerbino, S. Mazzoni, C. J. Takacs, D. S. Cannell, and M. Giglio, Nat. Commun. **2**, 290 (2011).
[32] A. Oprisan, B. Bayley, S. A. Oprisan, J. J. Hegseth, Y. Garrabos, C. Lecoutre, and D. Beysens, in *SPIE, Visual Information Processing XIX*, edited by Z.-u. Rahman, S. E. Reichenbach, and M. A. Neifeld (SPIE, Bellingham, WA, 2010).
[33] K. Hamano, S. Teshigawara, T. Koyama, and N. Kuwahara, Phys. Rev. A **33**, 485 (1986).
[34] M. L. Alessi, A. I. Norman, S. E. Knowlton, D. L. Ho, and S. C. Greer, Macromolecules **38**, 9333 (2005).
[35] G. T. Feke, G. A. Hawkins, J. B. Lastovka, and G. B. Benedek, Phys. Rev. Lett. **27**, 1780 (1971).
[36] J. J. Hegseth, V. S. Nikolayev, D. Beysens, Y. Garrabos, and C. Chabot, in *Fourth Microgravity Fluid Physics and Transport Phenomena* (NASA, Cleveland, OH, 1998).
[37] C. Lecoutre, Y. Garrabos, E. Georgin, F. Palencia, and D. Beysens, Int. J. Thermophys. **30**, 810 (2009).
[38] N. Komin and R. Toral, Physica D: Nonlinear Phenomena **239**, 1827 (2010).
[39] D. Beysens, A. Bourgou, and P. Calmettes, Phys. Rev. A **26**, 3589 (1982).
[40] R. Behrends, U. Kaatze, and M. Schach, J. Chem. Phys. **119**, 7957 (2003).
[41] P. Jany, Exp. Therm. Fluid Sci. **3**, 124 (1990).
[42] R. B. Kopelman, R. W. Gammon, and M. R. Moldover, Phys. Rev. A **29**, 2048 (1984).
[43] I. Iwanowski, A. Sattarow, R. Behrends, S. Z. Mirzaev, and U. Kaatze, J. Chem. Phys. **124**, 144505 (2006).
[44] F. J. Pearson, Proc. Phys. Soc. **75**, 633 (1960).
[45] E. S. R. Gopal, Resonance **5**, 37 (2000).
[46] D. S. Cannell, Phys. Rev. A **12**, 225 (1975).
[47] P. Jany and J. Straub, Int. J. Thermophys. **8**, 165 (1987).
[48] D. Beysens and G. Zalczer, Opt. Commun. **26**, 172 (1978).
[49] H. B. Tarko and M. E. Fisher, Phys. Rev. B **11**, 1217 (1975).
[50] B. Chu and W. P. Kao, Can. J. Chem. **43**, 1803 (1965).
[51] M. R. Moldover, J. V. Sengers, R. W. Gammon, and R. J. Hocken, Rev. Mod. Phys. **51**, 79 (1979).
[52] M. A. U. Anisimov, *Critical Phenomena in Liquids and Liquid Crystals* (Gordon and Breach Science Publishers, New York, 1991).
[53] A. L. Sengers, R. Hocken, and J. V. Sengers, Phys. Today **30**, 42 (1977).
[54] J. M. Ortiz de Zárate and J. V. Sengers, Phys. Rev. E **66**, 036305 (2002).
[55] M. Barmatz, I. Hahn, J. A. Lipa, and R. V. Duncan, Rev. Mod. Phys. **79**, 1 (2007).
[56] P. Guenoun, R. Gastaud, F. Perrot, and D. Beysens, Phys. Rev. A **36**, 4876 (1987).
[57] C. Houessou, P. Guenoun, R. Gastaud, F. Perrot, and D. Beysens, Phys. Rev. A **32**, 1818 (1985).
[58] R. Marcout, J. F. Zwilling, J. M. Laherrere, Y. Garrabos, and D. Beysens, Microgravity Quarterly **5**, 162 (1995).
[59] S. Bradbury and B. Bracegirdle, *Introduction to Light Microscopy* (BIOS Scientific Publishers, Oxford, UK, 2005).
[60] F. Zernike, Physica A: Statistical and Theoretical Physics **9**, 689 (1942).
[61] F. Zernike, Physica A: Statistical and Theoretical Physics **9**, 974 (1942).
[62] D. B. Murphy, *Fundamentals of Light Microscopy and Electronic Imaging* (John Wiley & Sons, New York, 2001).
[63] H. Harutyunyan, S. Palomba, J. Renger, R. Quidant, and L. Novotny, Nano Lett. **10**, 5076 (2010).
[64] Y. Jayalakshmi, B. Khalil, and D. Beysens, Phys. Rev. Lett. **69**, 3088 (1992).
[65] C. Morteau, M. Salzman, Y. Garrabos, and D. Beysens, in *2nd European Symposium on Fluids in Space*, edited by A. Viviani (Congressi srl, Rome, 1997).
[66] D. A. Beysens and Y. Garrabos, Physica A **281**, 361 (2000).
[67] C. Bartscher and J. Straub, Int. J. Thermophys. **23**, 77 (2002).
[68] E. D. Siggia, B. I. Halperin, and P. C. Hohenberg, Phys. Rev. B **13**, 2110 (1976).